RESEARCH

Size effects in the uniaxial compressive properties of 3D printed models of rocks: an experimental investigation

Hao Wu[1] · Yang Ju[2] · Xin Han[1] · Zhangyu Ren[3] · Yue Sun[1] · Yanlong Zhang[1] · Tianyi Han[1]

Abstract
Transparent physical models of real rocks fabricated using three-dimensional (3D) printing technology are used in photoelastic experiments to quantify the evolution of the internal stress and deformation fields of rocks. Therefore, they are rendered as an emerging powerful technique to quantitatively reveal the intrinsic mechanisms of rock failure. The mechanical behavior of natural rocks exhibits a significant size effect; however, limited research has been conducted on whether transparent physical models observe similar size effects. In this study, to make the transparent printed models accurately demonstrate the mechanical behavior of natural rocks and reveal the internal mechanism of the size effect in rock mechanical behavior, the size effect in 3D printed models of fractured and porous rocks under uniaxial compressive loading was investigated. Transparent cylindrical models with different sizes that contained different fractured and porous structures were printed using the fracture and porous characteristics extracted from natural coal and sandstone. The variation in uniaxial compressive strength and elastic modulus of fractured and porous models for increasing model sizes were obtained through uniaxial compression experiments. Finally, the influence of internal discontinuous structural features, such as fractures and pores, on the size effect pertaining to the mechanical behavior of the model was analyzed and elaborated by comparing it with the mechanical properties of the continuous homogeneous model without fractures and pores. The findings provided support and reference to analyze the size effect of rock mechanical behavior and the effect of the internal discontinuous structure using 3D printed transparent models.

1 Introduction

Surface subsidence, gas blow-out, rockburst, water inrush, and other disasters in production and development operations considerably restrict the safe and efficient development of underground mineral resources and damage the environment (Sun et al. 2021; Zhang et al. 2020). It is essential to scientifically understand and accurately describe the

triggering mechanism and control factors of the aforementioned engineering disasters for ensuring the green, low-carbon, and safe operation of mineral resources (Liu et al. 2021). However, natural rocks show significant discontinuities due to geological tectonic movements, corrosion, and unloading. The discontinuous structure of the rock causes its mechanical behavior changes with observational scales (i.e., the mechanical behavior of the rock shows a size effect). Numerous researchers have developed various experimental studies using natural rock samples to accurately characterize the intrinsic mechanism of the size effect of rock mechanical behavior. Based on various studies, the uniaxial compressive strength (UCS) of many rocks, including coal, granite, slate, and marble, were found to decrease for increasing rock sample size (Bieniawski 1968; Li et al. 2021; Rong et al. 2018; Song et al. 2018). Based on this phenomenon, many researchers established the rock size effect law using fracture mechanics, damage mechanics, and multiple fractals to determine a reasonable representative volume element

✉ Yang Ju
  juy@cumtb.edu.cn

1   School of Mechanics & Civil Engineering, China University
    of Mining &Technology (Beijing), Beijing 100083, China

2   State Key Laboratory of Coal Resources and Safe Mining,
    China University of Mining & Technology (Beijing),
    Beijing 100083, China

3   School of Emergency Management and Safety Engineering,
    China University of Mining & Technology (Beijing),
    Beijing 100083, China

(RVE) for rock samples in engineering calculation and design, and used the mechanical response of RVE-scale rock samples to analyze and predict the deformation damage of rocks at engineering scales (Carpinteri et al. 1995; Darbor et al. 2018; Ma et al. 2021; Shirole et al. 2020). Nevertheless, other studies have found the opposite phenomenon of size effect in rocks. For example, the UCS of rocks with large porosity, such as Hawkesbury sandstone and dissolved tuff, increases as the sample diameter increases (Pells 2004; Yuki et al. 1995). The sandstone and granite show a progression (increasing and then decreasing) of the UCS as the specimen size increases (Hawkins 1998; Masoumi et al. 2016; Quiñones et al. 2017; Zhai et al. 2020). Uniaxial compression experiments conducted by Thuro found no significant size effects on the UCS and elastic modulus of limestone and granite (Thuro et al. 2001). The aforementioned studies show that the internal discontinuous structure of rocks is a key factor affecting the size effect of rock mechanical behavior. However, there is still a lack of a deep understanding and accurate description of the internal discontinuous structure and its influence on rock mechanical behavior. Thus, it is difficult to scientifically capture and accurately predict the different size effect laws of rock mechanical behavior.

Recently, to explore the effect of internal discontinuous structures on mechanical behaviors, three-dimensional (3D) printing technology has created advantageous conditions for the preparation of complex structural models of rocks (Ju et al. 2019, 2017; Kong et al. 2018; Sharafisafa et al. 2018; Song et al. 2021; Xia et al. 2021). 3D printed models of rocks overcome the traditional problems that exist in the study of rock size effects, including difficult sampling, expensive, large differences in the internal structure of rocks, poor generalization of experimental results, and inaccessibility for comparison (Fereshtenejad and Song 2021; Ibrahim et al. 2021; Jiang and Zhao 2014). At present, various 3D printing technologies are widely used to prepare 3D-printed rock samples (Borrello et al. 2018; Espalin et al. 2014; Rajpurohit and Dave 2018), such as fused deposition modeling, stereolithography, and selective laser sintering. In particular, the application of light-sensitive resins, polylactic acid, and gypsum has opened up completely new avenues for studying the physical and mechanical properties of natural rocks with printed models (Ju et al. 2021; Yan et al. 2020). Numerous researchers have used 3D printing technology to prepare physical models that possess the same structure as natural rocks and investigated the differences between the physical and mechanical behaviors of these models and natural rocks (Gao et al. 2020; Kong et al. 2021, 2018; Mostaghimi et al. 2017; Schlüter et al. 2014; Zhou and Zhu 2017). Current rock 3D printing research focuses on the observation of the basic mechanical properties in the size range of representative samples (i.e., the mechanical properties at the RVE scale), and studies on the size effect of the

mechanical behavior of rock printed models and the RVE characteristic scale are limited. It is unclear whether rock 3D printed models exhibit a similar size effect as natural rocks. The effect of internal discontinuous structural features on the size effect of mechanical behavior and the RVE characteristic scale of printed models must be investigated.

To solve these problems and enable transparent printed models to accurately capture the mechanical behavior of natural rocks and reveal the intrinsic mechanism of the dimensional effect of rock mechanical behavior, this study used computed tomography (CT) imaging, 3D digital reconstruction, and 3D printing technology to print and prepare transparent cylindrical models of coal and sandstone with different sizes, containing different fractured and porous structures based on the fractured and porous structure information extracted from natural coal and sandstone. Moreover, uniaxial compression experiments using the cylindrical model were conducted to obtain the variation in UCS and elastic modulus of the fractured and porous model with the model size. Finally, the mechanical behavior of the model was compared with that of a homogeneous model without fractures and pores to demonstrate the size effects of internal discontinuous structures such as fractures and pores on the mechanical behavior. This study can serve as a reference for accurately understanding and quantitatively analyzing the size effect of the mechanical behavior of rocks.

2 Printed models and methods

2.1 Digital reconstruction of natural rocks

In this study, natural coal and sandstone containing a considerable amount of discontinuous structure were selected as rock samples, as shown in Figs. 1 and 2, respectively. Figure 1 shows a natural coal sample, containing well-developed cracks, obtained 700 m below the surface of the Shanjiaoshu coal mine in Guizhou Province, China. Figure 2 shows a naturally formed muddy coarse sandstone, acquired 1300 m below the surface in Ludong, Shandong Province, China, containing well-distributed pores. The natural core samples were cylindrical with a diameter of 25 mm and a height of 50 mm. Figures 1b–e and 2b–e show the construction process of digital models for coal and sandstone, respectively. To accurately identify and analyze the internal microstructure of the rocks, a microfocus X-ray CT scanning system was used to scan the entire cylinder at intervals of 10, obtaining rock CT scan images with an image resolution of 50 μm. To quantify and compare the effects of the internal discontinuities on the mechanical properties of the rocks and satisfy the accuracy requirements of the 3D-printing fabrication of the rock models, we selected a local part of well-developed fractures and pores that adequately represent

the internal structural characteristics of rocks to construct the RVE models shown in Figs. 1, 2, 3. The primary consideration of this strategy includes that it is impractical to get natural rock samples with similar internal discontinuities but various sizes. This facilitates comparing the mechanical properties of the rock models with similar discontinuities but various sizes. Moreover, it is technically difficult and economically expensive to get large-size real rock cores for testing the size effect of rock mechanical behavior. Using the RVE models generated from local representative discontinuities and their amplified samples can resolve this problem. Figures 1b–c and 2b–c show the CT images of the cross-section of the coal and sandstone samples and the extracted local structure. Then, the independently developed image processing and recognition program (Ju et al. 2013) was used to binarize the local structure images to

form binarized images of the fractured and porous structure within this cross-section, as shown in Figs. 1d and 2d, where the black part indicates the matrix of the rock sample and the white parts represent fractures and pores. Similarly, identical image processing and recognition methods were applied to the CT scan images of the local structures of each layer of the coal and sandstone samples to obtain the binarized images of the local structures of each layer. Finally, the Mimics® software (Ju et al. 2019) was applied to reconstruct all the local structure binarized images of each layer in 3D along the z-direction to obtain digital reconstruction models with the discontinuous structure of coal and sandstone, as shown in Figs. 1e and 2e. Furthermore, a smooth shell with a thickness of 1.0–1.5 mm was designed for the numerical model to fabricate a physical model with a discontinuous structure of coal and sandstone. It further maintains
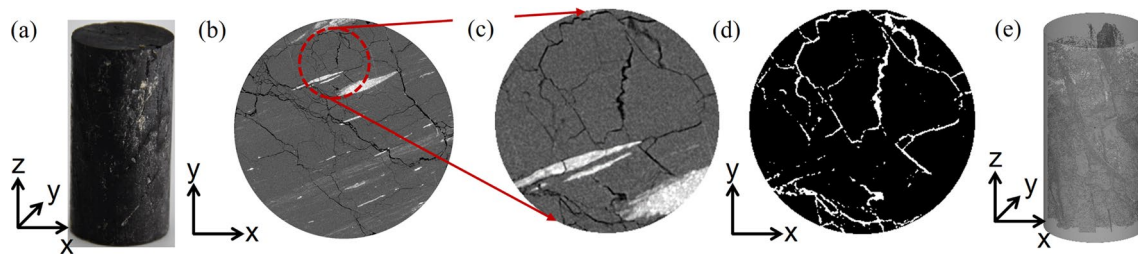

Fig. 1 Construction of digital fractured coal model. **a** Natural coal sample; **b–d** Extraction of discontinuous cracks in coal; **e** Digital model
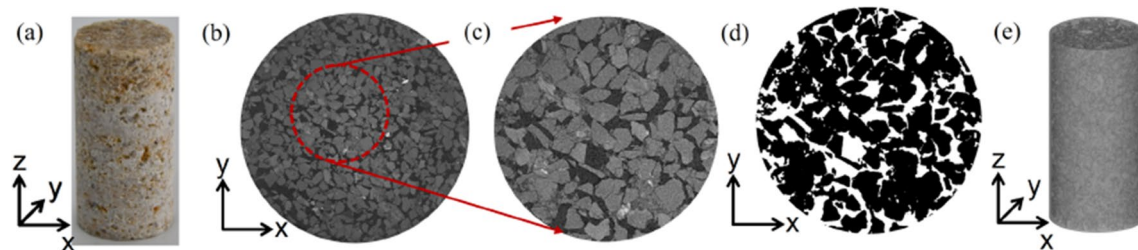

Fig. 2 Construction of digital porous sandstone model. **a** Natural sandstone sample; **b–d** Extraction of discontinuous pores in sandstone; **e** Digital model
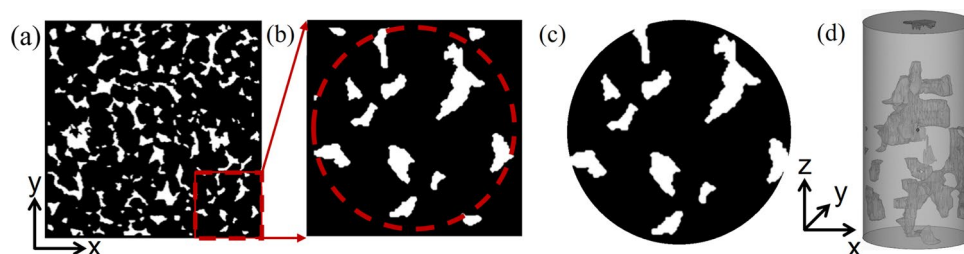

Fig. 3 Construction of digital Berea sandstone model with amplified pores. **a–c** Extraction of discontinuous pores in sandstone; **d** Digital model

the integrity of the model, and effectively bears the external load. Figures 1e and 2e show the 3D digital models of the fractured and porous structures that were constructed based on the microscopic information of the natural coal and sandstone. In addition, we selected CT scan images of the Berea sandstone provided by Imperial College London (Ju et al. 2019) and used a similar processing method to construct a set of numerical models with amplified pores to investigate the effect of different discontinuous structures on the size effect of the rock mechanical behavior, as shown in Figs. 3a–d. The influence of internal discontinuous pore structure features on the size effect of the model was studied by comparing the experimental results of the natural (Fig. 2e) and amplified (Fig. 3d) porous models.

2.2 Printed models of natural rocks

According to the theory of fracture mechanics (Bažant 1984 and 1997), for natural rocks, with increasing size, the morphological features and the distribution characteristics of the internal discontinuous structures change, which result in the size effect of rocks. In this study, to reveal the effect of the single factor, i.e., the scale of internal discontinuous structure, on the macroscopic mechanical behavior of the model, we only changed the ratio of specimen dimension to explore if the specimen will still exhibit size effect as the morphology of the internal discontinuous structure is same. Therefore, we designed a set of RVE models with equivalent scaling to ensure that the morphological features and distribution patterns of the discontinuities were similar for the RVE models of different sizes. We tested whether the

Table 1 Mechanical parameters of the printing material at room temperature (Ju et al. 2020)

Materials	Uniaxial tensile strength f_t (MPa)	Uniaxial compression strength f_c (MPa)	Elastic modulus E (GPa)	Poisson's ratio
Veroclear RGD 810	38.1	81.6	3.1	0.38

rock RVE models still exhibited size effects under identical morphological features. The 3D transparent physical models were prepared using a STRATASYS J750 3D printer. The 3D printer uses PolyJet technology to print layer by layer longitudinally with a thickness of up to 14 μm and the printing accuracy can reach 20–85 μm. The matrix part of the model was prepared by VeroClear RGD 810, which is a photosensitive material with high-stress photosensitivity and can simulate the hard and brittle properties of rocks (Song et al. 2021; Zhou and Zhu 2017). The structure of the model fractures and pores was replaced by the grid support material Fullcure705, which is a water-soluble material with a sparse structure and near-zero tensile and shear strength. Table 1 lists the basic mechanical parameters of the printed materials. The test details can be found in our previous studies (Ju et al. 2017, 2014). To minimize the effect of UV irradiation on the strength of different size models when they are cured, the models were printed in multiple batches, and only those with the same structure and the same size were printed in each batch. Considering that the deposition direction during the formation of natural rocks and the coring direction of natural rocks are parallel to the Z-axis (Wang et al. 2017), all models were printed layer by layer in the z-direction to avoid the impact of stack directions (see Fig. 4). Finally, four cylindrical models were printed (Fig. 5): homogeneous model (without discontinuous structure inside model), fractured model, porous model, and amplified porous model. The porosities of the porous model and amplified porous model were 21.7% and 4.6%, respectively. The four types of cylindrical models were scaled equivalently to compare and examine the size effect on the mechanical behavior of the models. The diameter×height of the specimens was 12.5 mm×25 mm, 25 mm×50 mm, 37.5 mm×75 mm, and 50 mm×100 mm. To obtain accurate experimental results, three identical specimens of each size model were printed for repeated testing. Simultaneously, three sizes of homogeneous models with diameters of 12.5, 25, and 50 mm were tested for a comparative analysis in this study due to the stable and regular mechanical properties of the homogeneous models that serve as a comparison (Foster et al. 2019; Prajzler et al. 2017; Rimington et al.
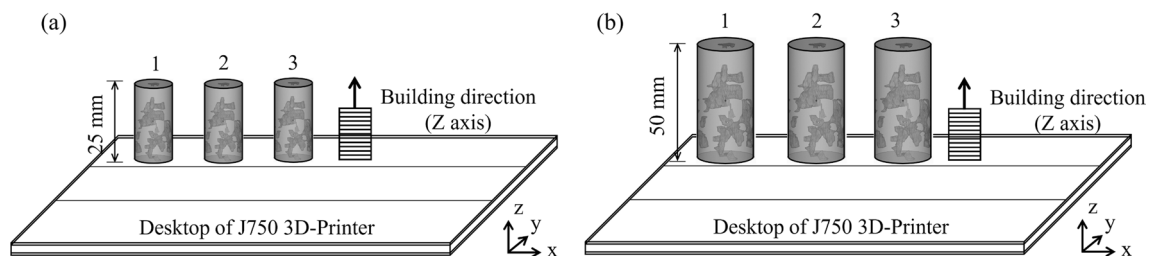

Fig. 4 Diagramatic representation of the printing process, showing the print direction and print batch. **a** Model height=25 mm; **b** Model height=50 mm
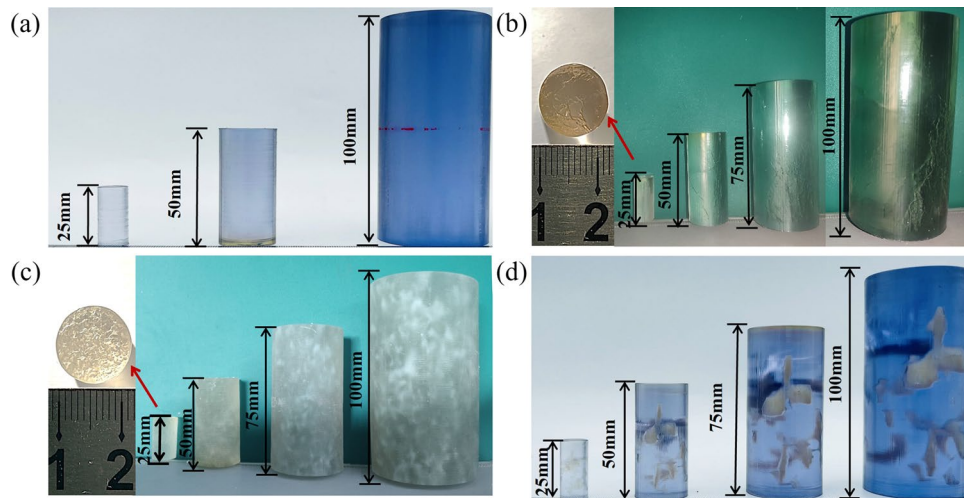
Fig. 5 Printed specimens of various sizes. **a** Homogeneous model; **b** Fractured model with real cleavages; **c** Porous model with real pores and **d** Porous model with amplified pores

2018). Finally, the models were maintained under dry conditions at room temperature (23 °C) for five days after printing to ensure that the printed models were completely cured to reach a stable state before conducting the experiments.

2.3 Experimental setup

The uniaxial compression experiments of the homogeneous, fractured, porous, and amplified porous models were carried out using the EHF-EG200KN full-digital hydraulic servo testing system. For an extensive comparison, using the ASTM D695 test standard, a strain rate of 0.5%/min was adopted. The quasi-static compression test was conducted at 23 °C for different sizes of specimens to compare the similarity of the experimental results from existing literature. The model was coated with petroleum jelly to eliminate the effect of frictional restraint between the loading end plate and the end of the model under pressure on the experimental result.
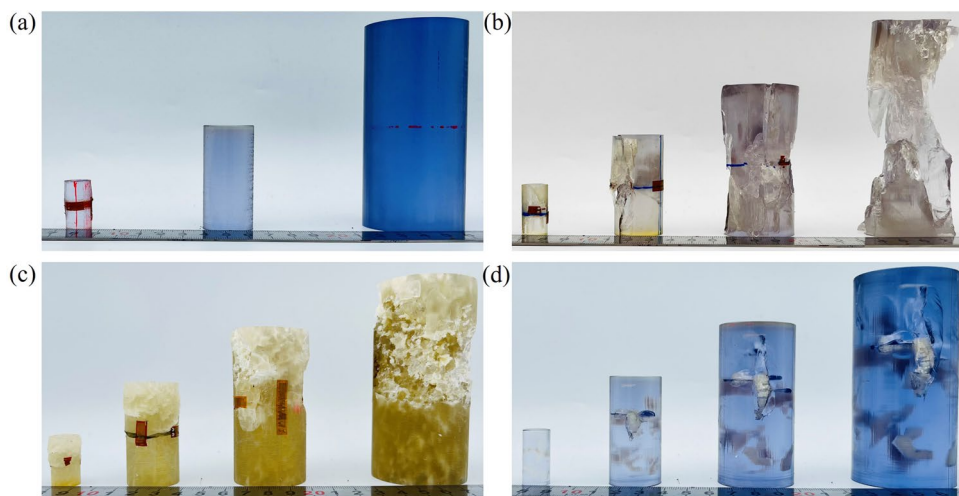

Fig. 6 Failure modes of different printed models. **a** Homogeneous model; **b** Fractured model with real cleavages; **c** Porous model with real pores; **d** Amplified porous model
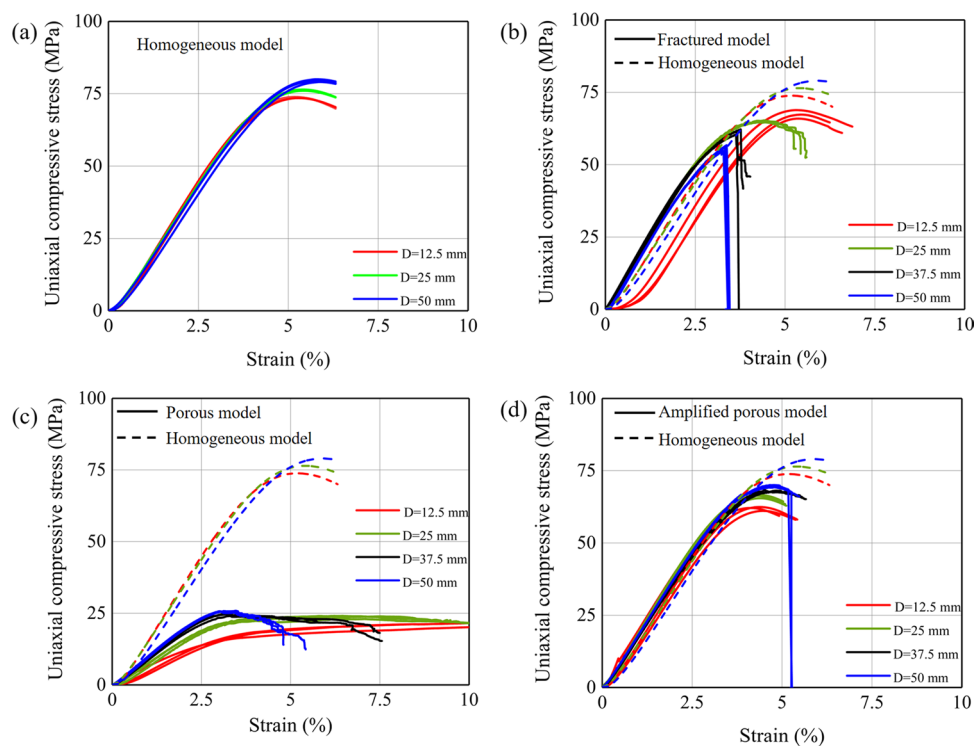
Fig. 7 Stress–strain curves of the printed models with and without internal discontinuous structures. **a** Homogeneous model; **b** Fractured model with real cleavages; **c** Porous model with real pores; **d** Amplified porous model

3 Results and discussions

This study summarizes and compares the mechanical behaviors, such as stress–strain response and failure modes of different models, and analyzes the influence laws of different discontinuous structures on the size effect of mechanical behaviors of printed models. The failure modes of the homogeneous, fractured, porous, and amplified porous models with different sizes are shown in Fig. 6. Figure 7 shows the compressive stress–strain curves of the homogeneous, fractured, porous, and amplified porous models with different sizes. The measured results of UCS and elastic modulus of the model with various sizes are summarized in Table 2. Figure 8 presents a comparison of the variation in UCS and elastic modulus with specimen size for different types of models. Finally, Fig. 9 shows the variation in UCS and modulus of elasticity with increasing model size for different types of models using the size model with a diameter of 12. 5 mm as a benchmark for comparison.

The results illustrate that the homogeneous model of different sizes exhibited plastic deformation characteristics and suffered large longitudinal compression and transverse expansion deformation under the action of axial compression, because the model exhibited no internal discontinuous structure and the Veroclear possessed high strength and strong plastic deformation capacity, as shown in Figs. 6a

and 7a. The UCS of the homogeneous model increased slightly for increasing model sizes, in which the UCS and elastic modulus of the model with a diameter of 50 mm only increased by approximately 7.86% and 7.84%, respectively, compared with the corresponding values of the model with a diameter of 12.5 mm. In addition, the stress–strain curves were close to each other and did not exhibit the size effect, which agrees with the size effect on the uniaxial compressive properties of dense homogeneous granite and limestone (Thuro et al. 2001); in other words, the uniaxial compressive performance of the model with uniform material and without discontinuous structure exerted no significant size effect in the range of RVE scales.

It was observed that the fractured models exhibited shear-brittle failure characteristics. The smaller size samples exhibited more evident plastic failure characters, which were accompanied by shear surfaces. The larger size samples showed more evident brittle splitting failure characters, and the failure mode was increasingly complex. The abruptness of the failure increased, along with the brittle characteristics, as shown in Figs. 6b and 7b. Evident differences were observed in the stress–strain curves of specimens of different sizes; at the beginning of loading, the stress–strain response of the model with a diameter of 12.5 mm remained in a nonlinear deformation phase; the initial cracks were compacted and closed without cracking extension, and the

Table 2 Measured uniaxial compressive strength (UCS) and elastic modulus (E) of the 3D printed models with various scales

Printed models	Diameter (mm)	UCS (MPa)	Average (MPa)	E (GPa)	Average (GPa)
Homogeneous model	12.5	73.88	73.73	2.55	2.55
		73.82		2.49	
		73.49		2.60	
	25	76.45	76.24	2.75	2.75
		76.02		2.76	
		/		/	
	50	79.05	79.53	2.68	2.75
		80.00		2.85	
		79.54		2.71	
Fractured model	12.5	65.92	67.37	1.94	2.01
		67.31		2.05	
		68.87		2.04	
	25	65.07	65.02	2.19	2.19
		65.32		2.22	
		64.67		2.15	
	37.5	61.38	61.32	2.16	2.13
		62.22		2.10	
		60.35		2.13	
	50	56.11	55.89	2.05	2.04
		56.74		2.05	
		54.82		2.01	
Porous model	12.5	/	15.2	0.59	0.63
		15.15		0.63	
		15.25		0.66	
	25	24.10	23.68	0.88	0.85
		23.94		0.86	
		23.00		0.84	
	37.5	25.21	24.76	1.08	0.99
		24.69		1.00	
		24.38		0.96	
	50	25.67	25.76	1.05	1.04
		25.9		1.02	
		25.71		1.05	
Amplified porous model	12.5	62.46	61.9	1.93	1.94
		62.12		1.93	
		61.11		1.87	
	25	65.49	66.13	1.99	2.00
		66.31		2.00	
		66.60		1.99	
	37.5	68.14	68.08	1.83	1.84
		67.83		1.83	
		68.27		1.85	
	50	70.05	69.68	1.91	1.92
		69.29		1.91	
		69.70		1.93	

model showed a highly apparent post-peak descent section when destroyed. Meanwhile, the UCS and peak strain of the model decreased as the size increased, and the non-linear deformation phenomenon disappeared. In addition, the initial internal fracture appeared to crack initially and expand. Therefore, the stress–strain response curve of the model showed an increasingly apparent elastic-brittle damage mode, in which the model with a diameter of 50 mm was damaged in the elastic section. The elastic modulus of the fractured model did not change significantly as the model

size increased, and the maximum difference was approximately 9%, as shown in Table 2 and Figs. 7b, 8b, and 9. Compared with the homogeneous model, the overall UCS of the fractured model decreased, as shown in Table 2 and Figs. 7b and 8a, which agrees with the conclusion that high-level defects during rock deformation failure play a decisive role in the mechanical properties of the model, as proposed by Feng (Feng and Zhao 2008).

Under the influence of pore size and distribution location, the porous model showed typical plastic failure
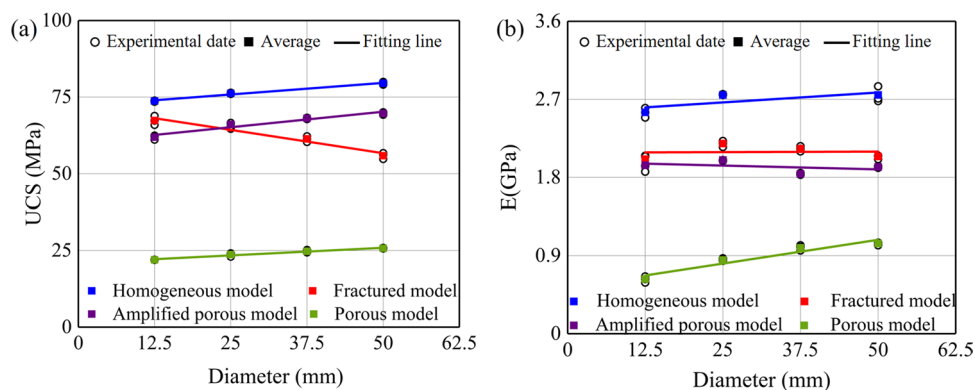
Fig. 8 Comparison of uniaxial compression mechanical properties of four types of printed models at varied scale sizes. **a** UCS and **b** Elastic modulus
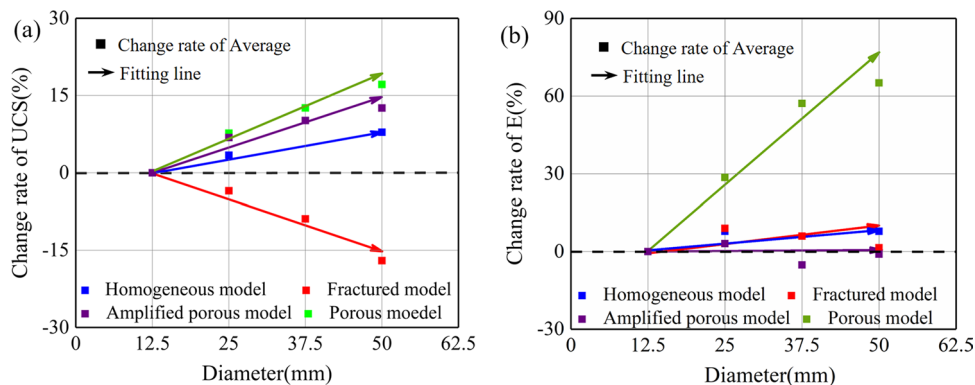

Fig. 9 Experimental results of the model with a diameter of 12.5 mm were used as a reference to quantify the size effect of the model with different internal structures. **a** UCS and **b** Elastic modulus

characteristics, and the plastic deformation failure characteristics gradually weakened as the model size increased. Furthermore, affected by local pores, the large-size model experienced sudden local failure and exhibited certain brittle failure characteristics, as shown in Figs. 6c and 7c. There were apparent size effects in the stress–strain curves of different sized models. First, at the initial stage of loading, the stress–strain responses of different size models showed an up-concave nonlinear deformation phase (i.e., the compacting phase, in which some micro-pores were compacted and closed without cracking). In the elastic phase, there was a significant difference in the slope of the stress–strain curves of the models of different sizes. Then, in the plastic stage, the models of different sizes showed stress plateau behavior, and the stress only decreased in a step-like pattern after the models produced large axial deformation. The appearance of the stress plateau was due to the plastic collapse of the pore wall inside the model at this stage after reaching a certain

plastic moment under load. The longitudinal strain continued to increase, and the stress showed a plateau behavior. As the size of the model increased, the peak strain decreased, peak strength increased, stress plateau decreased, and the post-peak stress–strain response gradually showed a brittle failure mode. The UCS and elastic modulus of the porous model gradually increased as the model size increased. Meanwhile, the smaller the internal pore size, the smaller the UCS, the larger the peak strain of the model, and the more significant the shaping characteristics of the stress–strain response, as shown in Table 2 and Figs. 7c, 8b, and 9. The overall compressive strength of the porous model was substantially decreased compared to the homogeneous and fractured models, as shown in Table 2 and Figs. 7c and 8a. The same results were observed in uniaxial compression experiments on natural highly porous sandstones (Fakhimi and Alavi 2011; Pells 2004).

The amplified porous model showed certain plastic deformation failure characteristics. The models of different sizes experienced collapse damage at the local pore volume location due to its distribution location and the influence of the local pore volume being amplified. However, the overall failure did not appear significantly, as shown in Figs. 6d and 7d. The stress–strain curves of the models with different sizes showed observable differences, however with no significant difference in the elastic modulus. As the model size increased, the UCS gradually increased and the peak strain decreased; the stress–strain response tended to experience brittle failure mode. The smaller the internal pore size, the smaller the V and the larger the peak strain. Moreover, the more significant the plastic characteristics of the stress–strain response, the closer to the response characteristics of the homogeneous model without discontinuous structure, as shown in Table 2 and Figs. 7d, 8b, and 9. Compared with the porous model, the overall compressive strength of the amplified porous model was substantially higher, however lower than that of the homogeneous model, as shown in Fig. 7d and Table 2.

The above experimental results indicate that the deformation failure mode, stress–strain response characteristics, UCS, peak strain, and the elastic modulus of homogeneous, fractured, porous, and amplified pore structures exhibited different size effect patterns as the model size increased, reflecting the mechanism of different influences of internal discontinuous structures on the size effect of the mechanical behavior of the printed model.

4 RVE scales for the size effects of various models

The results indicate that the 3D printed models of the rocks showed a similar size effect phenomenon to natural rocks. The variation pattern of the size effect was closely related to the discontinuous structure inside the model. It is necessary to determine the RVE characteristic scale of the size effect of the printed model and to develop a prediction model of the size effect of the printed model to quantify the physical and mechanical properties of natural rocks with discontinuous structures using the printed model. By combining the experimental results of this study, the widely used size effect model of natural rocks was adopted to characterize the size effect of the printed model and to determine the characteristic scale of the RVE of the printed model. From the perspective of the effects of particles inside the rock on the size effect, Hoek and Brown (1980) developed a model for calculating the strength size effect based on the strength of a cylinder with a diameter of 50 mm (Hoek and Brown 1980). Yoshinaka et al.

Table 3 The obtained parameters required in the FFSEL model for different printed samples

FFSEL parameters	σ_0 (MPa)	d_f	λd_0 (mm)
Fractured model	76.5	1.66	2.18
Porous model	76.5	2.22	0.047
Amplified porous model	76.5	2.14	0.467

(2008) validated the size effect model proposed by Hoek and Brown (1980) and modified the calculation model by considering the influence of rock type and the degree of weathering on the size effect (Yoshinaka et al. 2008). Based on fracture energy theory, Bažant (1984) assumed that the size effect of rock was caused by strain energy dissipation during macroscopic crack extension and proposed the size effect law (SEL, see Eq. (1)). Thereafter, Bažant (1997) proposed the fractal fracture size effect law (FFSEL, see Eq. (2)) based on the energy dissipation model of fractal cracks during extension (Borodich 1992; Mosolov and Borodich 1992).

$$\sigma_N = \frac{Bf_t}{\sqrt{1 + (d/\lambda d_0)}}, \tag{1}$$

$$\sigma_N = \frac{\sigma_0 \cdot d^{(d_f-1)/2}}{\sqrt{1 + (d/\lambda d_0)}}, \tag{2}$$

where σ_0 is strength for a sample with a negligible size that may be expressed in terms of intrinsic strength, d_f is the fractal dimension, σ_N is nominal strength, f_t is strength for a sample with the negligible size that may be expressed in terms of intrinsic strength, d_0 is maximum aggregate size, B and λ are dimensionless material constants, and d is the size of the specimen. Equations (1) and (2) explain and predict the SEL of rocks, which have been recognized by many rock mechanics practitioners.

The FFSEL model analyzed the endogenous mechanism of size effect for rocks based on fracture energy, which can be used for the analysis of the size effect and failure characteristics of elastic-brittle materials (e.g., rocks) and elastic–plastic materials (e.g., metals), together with the quantitative characterization and the prediction of the size effect of different structural models with the assistance of fractal theory. Consequently, in this study, FFSEL matches the experimental model and results. We quantitatively predicted the mechanical parameters of the fractured, porous, and amplified porous models using the FFSEL model and searched for a reasonable RVE characteristic size of the discontinuously printed rock model.
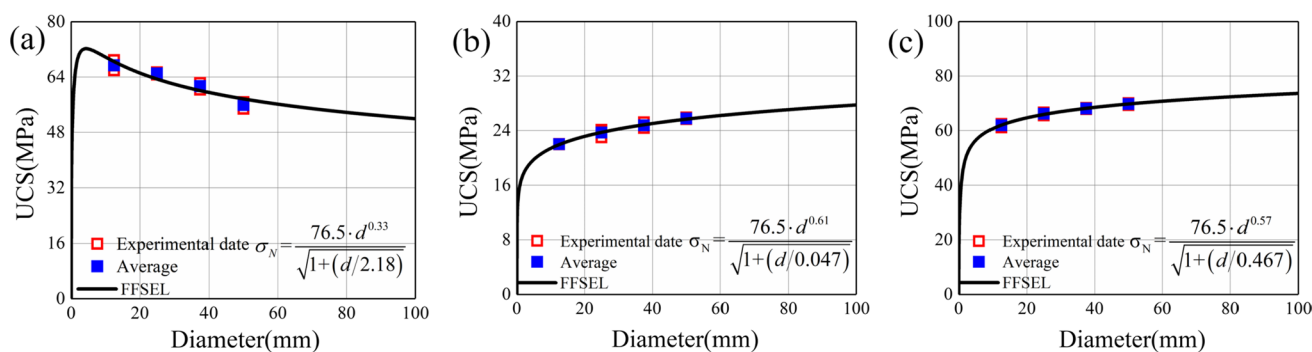
Fig. 10 FFSEL prediction results using the UCS data of the printed rock models. **a** Fractured model; **b** Porous model; **c** Amplified porous model

Table 3 lists the obtained parameters required for the FFSEL models for different printed samples, where σ_0 was set to 76.5 MPa, same with the strength of the homogeneous sample, according to the experimental results. Figure 10 shows the fitting results of the FFSEL models using the experimental data. The experimental data of all RVE models were fitted using the FFSEL model to determine the parameters required in the FFSEL model. The FFSEL prediction results and the experimental data were in good agreement, indicating that the printed RVE sample has a size effect consistent with the prototype rock. The size effect behavior of the discontinuous model was closely related to its internal discontinuous structure. Moreover, the size effect emerged from strain energy dissipation during the macroscopic crack expansion in the FFSEL model. There was no initial crack in the homogeneous model (i.e., the crack lengths are 0), and the failure mode showed plastic deformation characteristics without crack expansion. Therefore, there was no size effect in the UCS of the homogeneous model.

The fractal dimension d_f for the printed fractured, porous, and amplified porous specimens used in the FFSEL model were determined to be 1.66, 2.22, and 2.14, respectively. Meanwhile, experimental results showed that the three printed models failed by shear-brittle failure, plastic failure, and certain plastic deformation, respectively. Therefore, the main reason for the difference in the size effect between the fractured and porous models was as follows: the fractal characteristics of the fractured and porous models were significantly different due to the discontinuous structures, causing variations in the trend of energy dissipation rate during the failure of different structural models and eventually resulting in different strength size effects.

In short, there were differences in the RVE size of the porous and fractured models, and the effect law of the RVE size on the mechanical properties of the model must be considered in the relevant experiments.

5 Conclusions

In this study, the size effect of compressive strength and elastic modulus of transparent 3D-printed rock models under uniaxial compression was quantitatively analyzed and compared with the size effect of homogeneous models without any internal structure. In addition, we investigated the effect of the internal pore and the fracture structure of rocks on the size effect of transparent physical models of rocks. The main conclusions of this study are as follows:

(1) Transparent porous and fractured models that were consistent with the internal discontinuous structure of natural rocks, prepared through CT scanning and 3D printing techniques, could effectively resolve the size effect of the mechanical behavior of natural rocks.

(2) The deformation failure modes, stress–strain response characteristics, UCS, peak strain, and elastic modulus of the homogeneous, fractured, porous, and amplified porous structures exhibited different size effect patterns as the model size increased, which revealed the mechanisms with varying influences of the internal discontinuous structure on the size effect pertaining to the mechanical behavior of the printed model.

(3) Based on FFSEL, the mechanical behavior of the transparently printed model showed similar dimensional effects to natural rocks caused by strain energy dissipation during macroscopic crack expansion. In addition, the fractal characteristics of the discontinuous structure contributed to different experimental results.

Finally, we found that 3D printing could be used for fabricating small-sized discontinuous structures. However, owing to the lack of sufficient stiffness of the matrix material (E.g., Veroclear), the internal structure of the printed model under a loading state was compacted and showed a typical elastic–plastic state. Therefore, to avoid the stress

plateau phenomenon, rock printing model preparation must be considered from the size of the internal discontinuous structure.

Declarations

References

Bažant ZP (1984) Size effect in blunt fracture: concrete, rock, metal. J Eng Mech 110(4):518–535

Bažant ZP (1997) Scaling of quasibrittle fracture: hypotheses of invasive and lacunar fractality, their critique and Weibull connection. Int J Fract 83(1):41–65

Bieniawski ZT (1968) The effect of specimen size on compressive strength of coal. Int J Rock Mech Min Sci Geomech Abstr 5(4):325–335

Borodich FM (1992) Fracture energy of fractal crack propagated in concrete or rock. Dokl Akad Nauk SSSR 325(6):1138–1141

Borrello J, Nasser P, Iatridis J, Costa KD (2018) 3D printing a mechanically-tunable acrylate resin on a commercial DLP-SLA printer. Addit Manuf 23:374–380

Carpinteri A, Chiaia B, Ferro G (1995) Size effects on nominal tensile strength of concrete structures: multifractality of material ligaments and dimensional transition from order to disorder. Mater Struct 28(6):311–317

Darbor M, Faramarzi L, Sharifzadeh M (2018) Size-dependent compressive strength properties of hard rocks and rock-like cementitious brittle materials. Geosyst Eng 22(4):179–192

Espalin D, Muse DW, Macdonald E, Wicker RB (2014) 3D Printing multifunctionality: structures with electronics. Int J Adv Manuf Technol 72(5–8):963–978

Fakhimi A, Alavi Gharahbagh E (2011) Discrete element analysis of the effect of pore size and pore distribution on the mechanical behavior of rock. Int J Rock Mech Min Sci 48(1):77–85

Feng ZC, Zhao YS (2008) Control effect of fissure scale on deformation and failure of rock mass. Chin J Rock Mech Eng 27(1):78–83

Fereshtenejad S, Song JJ (2021) Applicability of powder-based 3D printing technology in shear behavior analysis of rock mass containing non-persistent joints. J Struct Geol 143:104251

Foster D, Corey C, Fisher C, Smith C, Paolella A (2019), Printed materials and their effects on quasi-optical millimeter wave guide lens systems. In: 2019 International solid freeform fabrication symposium

Gao YT, Wu TH, Zhou Y (2020) Application and prospective of 3D printing in rock mechanics: a review. Int J Miner Metall Mater 28(1):1–17

Hawkins AB (1998) Aspects of rock strength. Bull Eng Geol Env 57(1):17–30

Hoek E, Brown ET (1980) Underground excavations in rock. Institution of Mining and Metallurgy, London

Ibrahim ER, Jouini MS, Bouchaala F, Gomes J (2021) Simulation and validation of porosity and permeability of synthetic and real rock models using three-dimensional printing and digital rock physics. ACS Omega 6(47):31775–31781

Jiang C, Zhao GF (2014) A preliminary study of 3D printing on rock mechanics. Rock Mech Rock Eng 48(3):1041–1050

Ju Y, Xie HP, Zheng ZM, Lu JB, Mao LT, Gao F, Peng RD (2014) Visualization of the complex structure and stress field inside rock by means of 3D printing technology. Chin Sci Bull 59(36):5354–5365

Ju Y, Wang L, Xie HP, Ma GW, Zheng ZM, Mao LT (2017) Visualization and transparentization of the structure and stress field of aggregated geomaterials through 3D printing and photoelastic techniques. Rock Mech Rock Eng 50(6):1383–1407

Ju Y, Ren ZY, Li XL, Wang YT, Mao LT, Chiang FP (2019) Quantification of hidden whole-field stress inside porous geomaterials via three-dimensional printing and photoelastic testing methods. J Geophys Res Solid Earth 124(6):5408–5426

Ju Y, Wang YT, Ren ZY, Mao LT, Wang YL, Chiang FP (2020) Optical method to quantify the evolution of whole-field stress in fractured coal subjected to uniaxial compressive loads. Opt Lasers Eng 128:106013

Ju Y, Guo W, Ren ZY, Zheng JT, Mao LT, Hu X, Liu P (2021) Experimental study on mechanical and optical properties of printable photopolymer used for visualising hidden structures and stresses in rocks. Opt Mater 111:110691

Ju Y, Xing MX, Sun HF (2013) Computer program for extracting and analyzing fractures in rocks and concretes. Software Copyright Registration 530646.

Kong LY, Ostadhassan M, Liu B, Li CX, Liu KQ (2018) Multifractal characteristics of MIP-based pore size distribution of 3D-printed powder-based rocks: a study of post-processing effect. Transp Porous Media 129(2):599–618

Kong LY, Ishutov S, Hasiuk F, Xu CC (2021) 3D printing for experiments in petrophysics, rock physics, and rock mechanics: a review. SPE Reserv Eval Eng 24(04):721–732

Li KH, Yin ZY, Han DY, Fan X, Cao RH, Lin H (2021) Size effect and anisotropy in a transversely isotropic rock under compressive conditions. Rock Mech Rock Eng 54(9):4639–4662

Liu B, Zhao YX, Zhang C, Zhou JL, Li YT, Sun Z (2021) Characteristic strength and acoustic emission properties of weakly cemented sandstone at different depths under uniaxial compression. Int J Coal Sci Technol 8(6):1288–1301

Ma WL, Chen H, Zhang W, Tan C, Nie ZB, Wang J, Sun Q (2021) Study on representative volume elements considering inhomogeneity and anisotropy of rock masses characterised by non-persistent fractures. Rock Mech Rock Eng 54(9):4617–4637

Masoumi H, Saydam S, Hagan PC (2016) Unified size-effect law for intact rock. Int J Geomech 16(2):04015059

Mosolov AB, Borodich FM (1992) Fractal fracture of brittle bodies under compression. Dokl Akad Nauk SSSR 324(3):546–549

Mostaghimi P, Armstrong RT, Gerami A, Hu YB, Jing Y, Kamali F, Liu M, Liu ZS, Lu X, Ramandi HL, Zamani A, Zhang YL (2017) Cleat-scale characterisation of coal: an overview. J Nat Gas Sci Eng 39:143–160

Pells PJN (2004) On the absence of size effects for substance strength of Hawkesbury Sandstone. Aust Geomech 39(1):79–83

Prajzler V, Kulha P, Knietel M, Enser H (2017) Large core plastic planar optical splitter fabricated by 3D printing technology. Opt Commun 400:38–42

Quiñones J, Arzúa J, Alejano LR, García-Bastante F, Ivars DM, Walton G (2017) Analysis of size effects on the geomechanical parameters of intact granite samples under unconfined conditions. Acta Geotech 12(6):1229–1242

Rajpurohit SR, Dave HK (2018) Flexural strength of fused filament fabricated (FFF) PLA parts on an open-source 3D printer. Adv Manuf 6(4):430–441

Rimington RP, Capel AJ, Player DJ, Bibb RJ, Christie SDR, Lewis MP (2018) Feasibility and biocompatibility of 3D-printed photopolymerized and laser sintered polymers for neuronal, myogenic, and hepatic cell types. Macromol Biosci 18(7):1800113

Rong G, Peng J, Yao MD, Jiang QH, Wong LNY (2018) Effects of specimen size and thermal-damage on physical and mechanical behavior of a fine-grained marble. Eng Geol 232:46–55

Schlüter S, Sheppard A, Brown K, Wildenschild D (2014) Image processing of multiphase images obtained via X-ray microtomography: a review. Water Resour Res 50(4):3615–3639

Sharafisafa M, Shen LM, Xu QF (2018) Characterisation of mechanical behaviour of 3D printed rock-like material with digital image correlation. Int J Rock Mech Min Sci 112:122–138

Shirole D, Walton G, Hedayat A (2020) Experimental investigation of multi-scale strain-field heterogeneity in rocks. Int J Rock Mech Min Sci 127:104212

Song HH, Jiang YD, Elsworth D, Zhao YX, Wang JH, Liu B (2018) Scale effects and strength anisotropy in coal. Int J Coal Geol 195:37–46

Song R, Wang Y, Sun SY, Liu JJ (2021) Characterization and micro-fabrication of natural porous rocks: from micro-CT imaging and digital rock modelling to micro-3D-printed rock analogs. J Petrol Sci Eng 205:108827

Sun YJ, Zuo JP, Karakus M, Liu L, Zhou HW, Yu ML (2021) A new theoretical method to predict strata movement and surface subsidence due to inclined coal seam mining. Rock Mech Rock Eng 54(6):2723–2740

Thuro K, Plinninger RJ, Zäh S, Schütz S (2001) Scale effects in rock strength properties. Part 1: unconfined compressive test and Brazilian test. ISRM regional symposium, EUROCK, pp 169–174

Wang L, Ju Y, Xie HP, Mao LT (2017) The mechanical and photoelastic properties of 3D printable stress-visualized materials. Sci Rep 7(1):1–9

Xia YJ, Meng QK, Zhang CQ, Liu N, Zhao ZX, Chen J, Yang G, Wang Y (2021) Application of 3D printing technology in the mechanical testing of complex structural rock masses. Geofluids 2021:1–23

Yan MM, Guo L, Cai P, Huang YM, Zhang QM, Lue QT (2020) Hydrothermal synthesis of NaYF4:Yb3+, Tm3+ upconversion microparticles and their effects on polymerization for stereolithography. Opt Mater 109:110311

Yoshinaka R, Osada M, Park H, Sasaki T, Sasaki K (2008) Practical determination of mechanical design parameters of intact rock considering scale effect. Eng Geol 96(3–4):173–186

Yuki N, Aoto S, Ogata Y, Yoshinaka R, Terada M (1995) The scale and creep effects on strength of welded tuff. In: Yoshinaka R, Kikuchi K (eds) International workshop on rock foundation. Balkema, Tokyo

Zhai H, Masoumi H, Zoorabadi M, Canbulat I (2020) Size-dependent behaviour of weak intact rocks. Rock Mech Rock Eng 53(8):3563–3587

Zhang DX, Guo WY, Zang CW, Gong XF, Li ZH, Qiu Y, Chen WG (2020) A new burst evaluation index of coal–rock combination specimen considering rebound and damage effects of rock. Geomat Nat Haz Risk 11(1):984–999

Zhou T, Zhu JB (2017) Identification of a suitable 3D printing material for mimicking brittle and hard rocks and its brittleness enhancements. Rock Mech Rock Eng 51(3):765–777